European Journal of Mechanics / A Solids 91 (2022) 104424

Contents lists available at ScienceDirect

European Journal of Mechanics / A Solids

journal homepage: www.elsevier.com/locate/ejmsol

Creep crack growth modelling of Grade 91 vessel weldments using a modified ductility based damage model

Raheeg Ragab [a,**], Jonathan Parker [b], Ming Li [c,***], Tao Liu [a,*], Wei Sun [a]

[a] Faculty of Engineering, University of Nottingham, Nottingham, NG7 2RD, UK
[b] Electric Power Research Institute, Charlotte, NC, USA
[c] School of Mechanics, Civil Engineering and Architecture, Northwestern Polytechnical University, China

ARTICLE INFO

Keywords:
Creep crack growth
Damage Mechanics
Ductility exhaustion
Vessel tests
Weldments

ABSTRACT

This paper reports creep crack growth modelling of Grade 91 vessel weldments at high temperature using a modified ductility-based continuum damage mechanics (CDM) model, which is based on the Kachanov-Rabotnov CDM and utilizing the concept of ductility exhaustion. The proposed model holds a key advantage over existing models in that it requires fewer material constants to be identified and calibrated. The new modified model was implemented into a user-defined subroutine in ABAQUS and then used to predict the creep crack growth of Grade 91 vessel weldments. Creep crack initiation and growth in the vessels were predicted to occur in the heat-affected zones of the weldments associated with the end closures, which is in good agreement with the corresponding vessel tests. Further, the predicted creep rupture lives of the notched bars and the vessels using the proposed model correlated reasonably well against the experimental results. This suggests that the modified ductility-based damage model can be used for creep crack growth and life prediction for high temperature structures with confidence.

1. Introduction

With the increasing derive to enhance the thermal efficiency and reduce carbon emissions, energy conversion systems such as power plants are expected to operate under high temperature and pressure conditions. Creep Strength Enhanced Ferritic (CSEF) steels including 9–12%Cr steels have been extensively used in the construction of high-energy components owing to their good mechanical performance, such as creep strength and oxidation resistance (Masuyama, 1999; Choudhary and Palaparti, 2012). When components operate under high-temperature creep regime, creep deformation and fracture are major concerns (Xu et al., 2017). As such, more reliable creep damage and creep life assessment methods are needed for safe, efficient and reliable plants operation.

Continuum damage mechanics-based models have been widely utilized for creep damage and creep life predictions. Typically, these methods can characterise the full creep stages and can be easily implemented into a finite element (FE) code to predict creep deformation and damage behaviour of steels at high temperatures (e.g., ref (Hayhurst et al., 1984; Hyde et al., 2004; Hyde et al., 2006)). In general, damage evolution models can be broadly categorised into stress-based and strain-based damage models (Wen et al., 2016). In the first category, the evolution of damage is based on the rupture (representative) stress criterion, while the latter approaches assume that material failure at a given point occurs when the locally accumulated creep strain reaches its critical value (i.e. creep ductility of the material) (Wen et al., 2016; Meng and Wang, 2019).

Stress-based damage evolution models (e.g. Kachanov-Rabotnov CDM (Kachanov, 1958; Rabotnov, 1969) and Liu-Murakami model (Liu and Murakami, 1998)) have been applied by many researchers to investigate creep damage and crack growth behaviour in high-temperature steels (Hyde et al., 2001) and damage induced by creep-fatigue conditions (Li et al., 2016). For instance, Hyde et al. (2001) have proposed a stress-based damage mechanics approach to predict creep damage initiation and growth in power plant steels weldment. Further, they presented an approach to determine material properties of the damage model based on accelerated creep tests (Hyde et al., 2001; Hyde and Sun, 2000). Goyal et al. (2013) successfully

* Corresponding author.
** Corresponding author.
*** Corresponding author.
E-mail addresses: Raheeg.Ragab@nottingham.ac.uk (R. Ragab), ming.li1@nwpu.edu.cn (M. Li), Tao.Liu@nottingham.ac.uk (T. Liu).

https://doi.org/10.1016/j.euromechsol.2021.104424
Received 3 April 2021; Received in revised form 30 August 2021; Accepted 22 September 2021
Available online 25 September 2021

predicted creep deformation and damage evolution in 2.25Cr–1Mo steels under uniaxial and multiaxial creep conditions by performing FE analysis coupled with stress-based continuum damage models. A novel approach has been presented by Hyde, C.J et al. (Hyde et al., 2010a) for modelling creep crack growth of 316 stainless steel using continuum damage mechanics, in conjunction with the finite element (FE) methods. The predicted crack patterns were consistent with the experimental observations. Similar work has been used to model the high-temperature creep damage and crack growth in P91 steel weldments through the applications of stress-based CDMs (Hyde et al., 2010b, 2010c). In a recent study by the author (Ragab et al., 2021), a multi-axial creep damage model of Kachanov type was adopted to investigate the creep failure behaviour of a Grade 91 header weldment. The damage evolution is represented through stress-based formulations and found to produce consistent results (Ragab et al., 2021). Further examples on the stress-based creep damage modelling are provided in the cited references (Shlyannikov and Tumanov, 2018a; Hosseini et al., 2013; Naumenko and Kostenko, 2009; Xu and Barrans, 2003; Dyson, 2000; Pétry and Lindet, 2009). In summary, the application of stress-based CDMs have been successful in these investigations and critical findings regarding the damage locations, remaining life and failure mechanisms in high-temperature steels have been concluded. Nevertheless, stress-based continuum damage models require, in general, many material constants to be obtained. For instance, seven material constants should be identified in Kachanov type CDM (Hyde et al., 2001; Hyde and Sun, 2000), (e.g. A, n, m, B, φ, χ, α) and more than five material parameters are required in Liu-Murakami model (Liu and Murakami, 1998) and Dyson's model (Dyson, 2000). In addition, it has been found that a small change in the multi-axial parameter (α), which is typically used to define stress rupture criterion in stress-based CDMs, could lead to a significant change in the predicted creep rupture life and creep crack growth predictions of a P91 weldment (Hyde et al., 2010b; Hyde et al., 2010c) and therefore this parameter should be carefully calibrated. Most importantly, stress-based CDMs do not usually consider the effects of creep ductility on creep performance of metallurgically susceptible steels such as Grade 91 steels. As such, the wide variability observed in the creep performance of CSEF steels weldment cannot be adequately captured (Parker, 2017). It has been experimentally demonstrated that creep ductility has serious implications on the creep performance of CSEF steels at high temperatures (Parker, 2017; Parker and Siefert, 2018; Siefert, 2019; Holdsworth, 2019). Furthermore, experimental studies on CSEF steels have revealed that low ductility materials could exhibit creep life reductions under multi-axial stress state (Parker, 2017) and could also be at risk when metallurgical constraints due to weldments are present (Parker and Siefert, 2018; Siefert, 2019). Therefore, considerations of the creep ductility of specific heats are critical for creep damage predictions and crack growth analysis of steels at high temperatures.

Strain-based models, on the other hand, are based on the ductility exhaustion concept, where the rate of creep damage accumulation is defined as the ratio of the equivalent creep strain rate to material creep ductility (Yatomi et al., 2003; Nikbin et al., 1984). Several ductility-based damage models have been proposed in recent years to predict creep crack growth and damage in creeping solids with different levels of accuracy (e.g., ref (Nikbin et al., 1984; Cocks and Ashby, 1980; Wen and Tu, 2014; Zhang et al., 2017; Spindler, 2004; Nikbin, 2017)). Provided appropriate knowledge of strain accumulation is available, the strain-based models can yield more accurate life predictions than the stress-based damage evolution models (Wen et al., 2016; Spindler, 2007). For example, Cocks and Ashby (1980) proposed a multi-axial creep ductility-based model assuming that cavity growth is governed by the power law creep. This model has been widely used to investigate creep damage behaviour of steels and the related failure mechanisms (Shlyannikov and Tumanov, 2018b; Oh et al., 2011; Kim et al., 2013; Alang and Nikbin, 2018). Yatomi et al. (2008) developed a strain-based approach to predict creep crack growth in 316H stainless steel at 550 °C. Further, two-dimensional elastic–plastic–creep analyses are carried out under plane stress and plane strain conditions assuming power-law creep behaviour and using average creep strain rate to characterise the constitutive behaviour of the steel (Yatomi et al., 2008). While the predictions were found in reasonable agreement with the experimental data of 316H stainless steel, the applicability of this model for materials which tend to develop enhanced creep rates due to the accumulation of damage could be limited. Therefore, for materials with complex damage mechanisms such as CSEF steels, the damage evolution and creep deformation laws should couple each other. Wen et al. (2013) developed a novel creep damage model which accounts for the effects of creep damage and stress state on creep deformation. The model is employed into a FE code to simulate creep crack growth and damage in 316 stainless steel at 600 °C and the predicted results showed good correlations with the corresponding experimental results. However, the primary creep effects are ignored in the model proposed. For some materials, the primary creep can be significant and hence the time exponent in the time-hardening creep law (m) is not necessarily equal to zero (Hyde et al., 2004; Chang et al., 2015). Therefore, for more accurate assessments, creep damage evolution models should incorporate all stages of creep (primary, secondary and tertiary), which will be addressed in the new proposed model of this work. To overcome the key limitations presented above for stress- and strain-based damage evolution models, a modified strain-based continuum damage model on the basis of Kachanov-Rabotnov CDM is proposed in this work utilizing the concept of ductility exhaustion. The proposed model requires fewer material constants to be identified and calibrated comparing with that of Kachanov-Rabotnov. Further, the model characterises the full creep curve and enables the effects of creep rupture ductility on creep lives to be assessed.

In this study, a modified ductility-based continuum damage mechanics model is proposed to study creep crack growth behaviour of Grade 91 vessels weldment. The paper is laid out as follows: Section 2 presents a summary of the experimental data pertinent to creep tests on weldment and the results related to the long-term creep tests of the Grade 91 vessels. In Section 3, the modified ductility-based CDM model is presented and discussed. In Section 4, the optimization procedure adopted to determine material properties of the new model is illustrated. The capability of the proposed CDM model to predict creep damage and failure is examined in Section 5. Finally, concluding remarks and some insights into future work are presented in Section 6.

2. Experimental work

In this section, the main findings from creep tests are presented. The experimental data relevant to the accelerated creep tests on weldment (based metal, weld metal, heat-affected zone) are presented in Section 2.1, while those obtained from the long-term creep tests on Grade 91 vessels are reported in Section 2.2.

2.1. Creep tests on weldment

Accelerated creep tests were performed on Grade 91 weldment at a temperature of 625 °C to study the creep behaviour of these weldments under both uniaxial and multiaxial stress states. Further, the results related to these tests will be utilized to determine creep damage properties in the constitutive equations for each weld constituent (based metal, weld metal, heat-affected zone) as outlined in Section 4. The tested materials were extracted from an ex-service header, which was operating under a nominal steam temperature of 570 °C and internal pressure of 16.5 MPa for about 78,000 h. Further details on the ex-service header and its in-service behaviour are documented in the cited references (Review of Fabrication and, 2013; Parker and Brett, 2013). The experimental work was undertaken based on EPRI guidelines and ASTM standard methods, e.g. ASTM E2714-09. Details of the testing have been provided previously (Siefert, 2019; Takahashi et al., 2019), so

Table 1
Summary of plain bar and notched bar creep rupture tests for the BM and simulated HAZ (Siefert, 2019; Takahashi et al., 2019).

Material	Test	Temperature (°C)	Stress (MPa)	Rupture time (hours)
BM	Plain Bar	625	80	19703.0
			100	2982.3
			120	233.3
			160	27.3
	Notched Bar		100	19550.3
			120	7715.9
			160	1121.1
Simulated HAZ	Plain Bar	625	60	1953.0
			80	231.0
	Notched Bar		60	15544.4
			80	3475.4
			100	352.8

a summary of the main results obtained from the uniaxial, notched bar and cross-weld (CW) creep tests is presented in the following subsections.

2.1.1. Uniaxial creep tests and notched bar creep rupture tests

Uniaxial creep deformation and creep rupture data were measured by performing a total of six uniaxial creep tests at 625 °C and under a stress range of 80–160 MPa for the P91 BM, while the simulated HAZ was subjected to a stress range of 60–80 MPa. The terminology of simulated HAZ refers to a specific weld region generated from the application of simulated welding thermal cycles to replicate the mechanical and microstructural properties of the real HAZ (Takahashi et al., 2018). In the simulation process, specimens are heated at a rate of 1 °C/s for a peak temperature of 900 °C followed by a rapid cooling using Gleebe simulator, reproducing the partially transformed (PT) region in the HAZ. Following the simulation process, a post weld heat treatment (PWHT) is applied where the simulated HAZ samples are heated in an electrical furnace to 740 °C for about 4 h before gradually cooled. Further, six notched bar creep rupture tests were performed at 625 °C and under nominal stress (on the minimum notched cross-section) within the range 100–160 MPa for the base metal and 60–100 MPa for the simulated HAZ to evaluate the creep response of these materials under a multiaxial stress state. The experimentally measured failure times of the uniaxial creep tests and notched bar creep rupture tests are listed in Table 1. Fig. 1a shows the experimental uniaxial creep curves (nominal strain *vs* time) for the P91 BM under a stress of 80 MPa and for the simulated HAZ under 60 MPa.

2.1.2. Cross-weld creep tests

The creep behaviour of the Grade 91 weldment under high-temperature conditions was investigated using feature type cross-weld creep tests. For this purpose, two cross-weld specimens were manufactured from the Grade 91 weldment, comprising three different materials: BM, WM and HAZ. Both cross-weld specimens were tested at 625 °C and under two nominal stress (on the cross-section of the uniform section) levels of 60 MPa and 80 MPa. Table 2 provides a summary of the main results obtained from the cross-weld creep tests, while the creep curves are shown in Fig. 1b.

2.2. Long-term creep tests of the Grade 91 vessels

Long-term creep tests were conducted on two Grade 91 vessels manufactured from an ex-service header by (Parker and Siefert, 2020). The general layouts of the welded vessels are shown schematically in Fig. 2 and Fig. 3. Both vessels comprise cylindrical sections with an outside diameter of 457 mm and a wall thickness of 53 mm.Vessel-1 involves a hemispherical end cap, one original girth weld, two rows of stubs with six stubs per row, endplate closure, and the new weld joining the endplate, as shown in Fig. 2. Vessel-2 (shown in Fig. 3) comprises a longitudinal seam weld, one original girth weld, two rows of stubs with six stubs per row, end plug weld, endplate fitting, and the new weld joining the endplate.

Both vessels were creep tested at 625 °C and internal pressure of 15 MPa, following EPRI guidelines (Parker and Siefert, 2020). The tests provided key information on the effects of end closures and the associated weldment on the long-term high-temperature creep behaviour of the vessel components. Vessel-1 failed after 10,000 h and cracking was observed in the HAZ region on the endplate side of the weld, while vessel-2 lasted for approximately 8000 h and cracking was associated in general with the endplate fitting weld and end plug weld. The endplate

Table 2
Summary of cross-weld creep tests (Siefert, 2019).

ID	Temperature (°C)	Stress (MPa)	Rupture time (hours)	Failure location
CW-A	625	60	18270.3	Heat-affected zone
CW-B	625	80	5518.7	Heat-affected zone

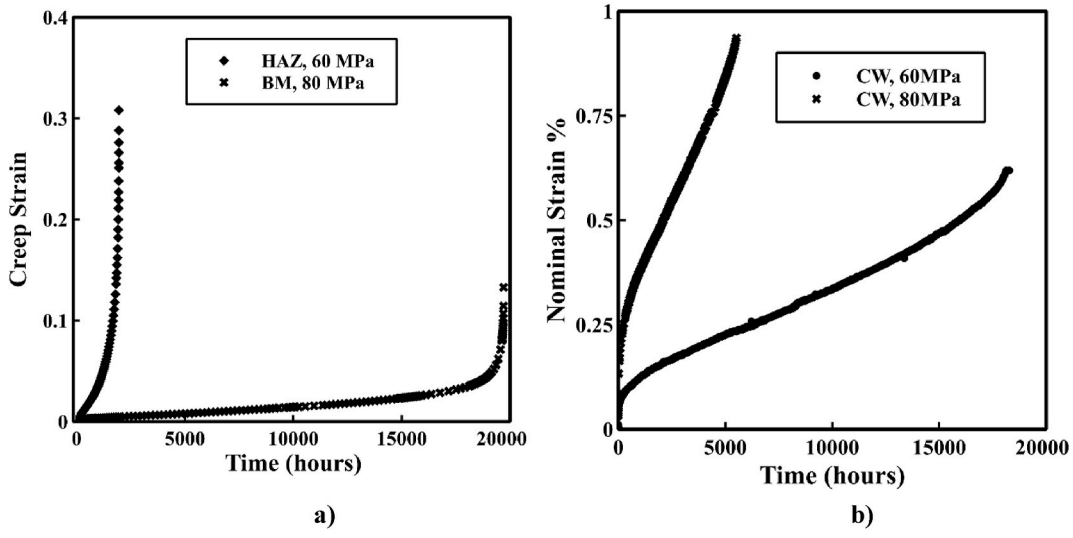

Fig. 1. Experimental creep curves at 625 °C for: a) the P91 BM under a stress of 80 MPa and for the simulated HAZ under 60 MPa, and b) the cross-weld specimens.

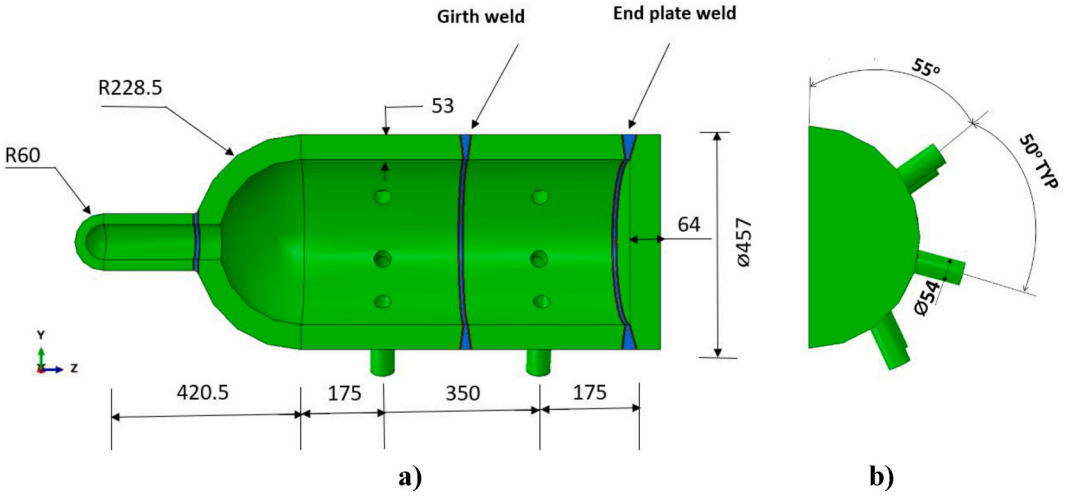

Fig. 2. Layout and dimensions of Vessel-1 on a) elevation view and b) side view (All dimensions in mm).

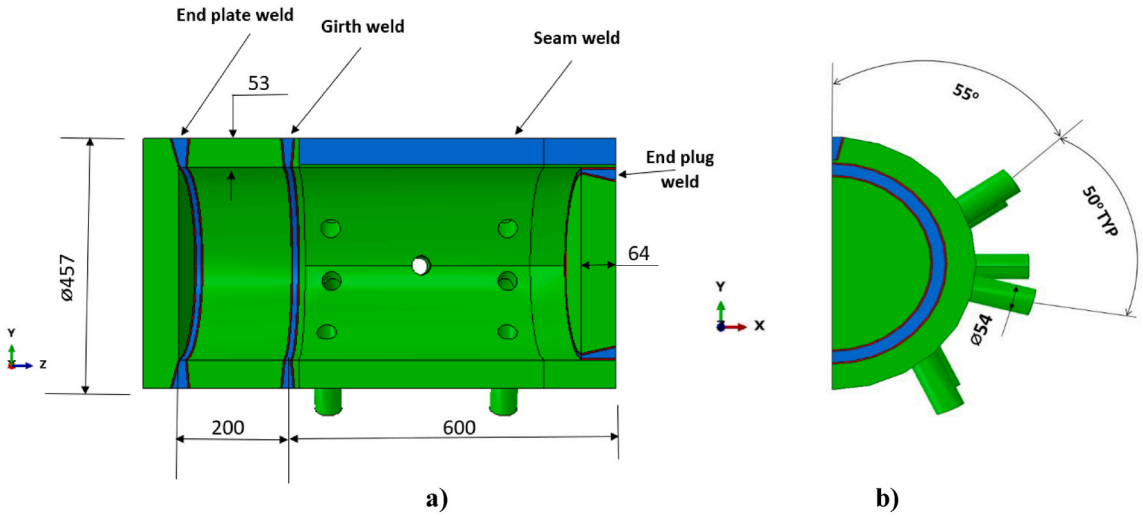

Fig. 3. Layout and dimensions of Vessel-2 on a) elevation view and b) side view (All dimensions in mm).

weld of vessel-2 developed cracks in the HAZ on the endplate side of the weld while the end plug weld cracking was confirmed in the HAZ on the header side of the weld. It should be noted that no cracking was detected for the girth weld or the longitudinal seam weld. Further details on the experimental work could be found in the cited reference (Parker and Siefert, 2020).

3. Constitutive models

In this section, a strain-based CDM model is proposed based on the classical Kachanov type CDM and utilizing the concept of ductility exhaustion. The constitutive equations (outlined in Section 3.1) are first expressed in the general multi-axial form. Then, a closed-form (analytical) solution is derived for creep strain as a function of time and for creep rupture life under uniaxial stress state. The multi-axial creep ductility is computed based on constrained void growth models, as outlined in Section 3.2.

3.1. Ductility-based creep damage constitutive equations

Kachanov type CDM (Kachanov, 1958; Rabotnov, 1969) is an empirical model, which incorporates a single state variable representing material damage due to internal cavitation, with a value ranges from 0 to 1, corresponding to no damage state and full damage state, respectively. The application of this model for examining creep deformation and fracture behaviour of power plant steels weldment has been successful in many previous investigations (e.g., ref (Hyde et al., 2004; Hyde et al., 2001)). The model can generally be expressed in the following multi-axial form:

For creep strain rate:

$$\frac{d\varepsilon_{ij}^{c}}{dt} = \frac{3}{2}A\left(\frac{\sigma_{eq}}{1-\omega}\right)^{n}\frac{S_{ij}}{\sigma_{eq}}t^{m} \tag{1}$$

Traditionally, in stress-based models, creep damage evolution is expressed in terms of the rupture stress as shown below:

$$\frac{d\omega}{dt} = B\frac{\sigma_{r}^{\chi}}{(1-\omega)^{\varnothing}}t^{m} \tag{2}$$

where the rupture stress is usually assumed to be a combination of the maximum principal stress and von-mises equivalent stress:

$$\sigma_{r} = \alpha\sigma_{1} + (1-\alpha)\sigma_{eq} \tag{3}$$

where S_{ij} and ε_{ij}^{c}, (i, j = 1,2,3) are the deviatoric stress and creep strain components, respectively; σ_{eq}, σ_1 and σ_r are the equivalent, maximum principal and rupture stresses, respectively; ω is a state variable

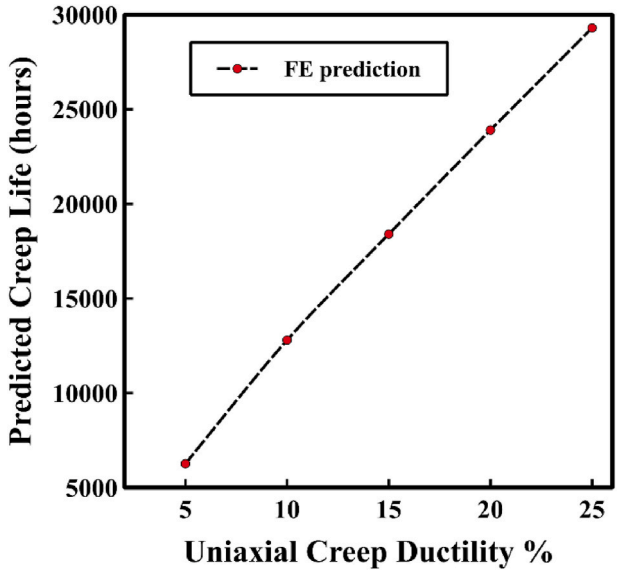

Fig. 4. Predicted creep rupture lives of Grade 91 notched bars at 625 °C and net section stress 100 MPa with different creep ductility values using the proposed model.

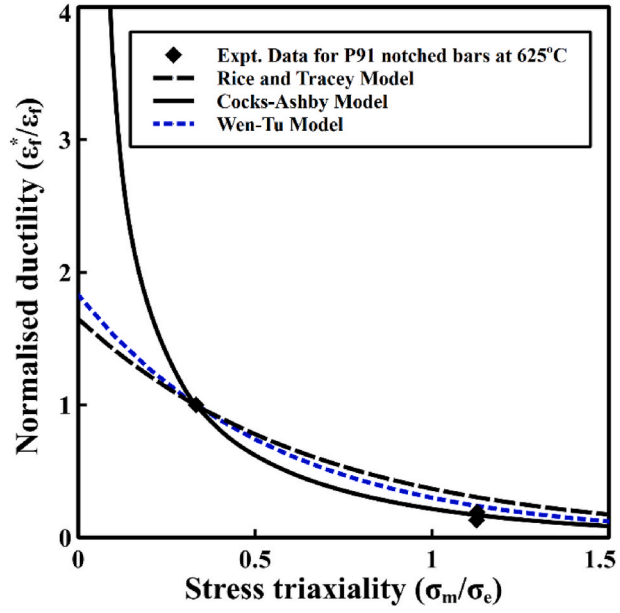

Fig. 5. Comparison of creep ductility predictions by several multiaxial constraint ductility models with the experimental data from plain and notched bar creep tests at 625 °C.

characterising creep damage due to internal cavitation, $\omega \in [0, 1]$; A, n, m, B, ∅, χ are the material constants related to the uniaxial stress sate.

Although the application of the stress-based damage mechanics models has been successful in many situations, there are key limitations including the larger number of material constants to be calibrated, as shown above. Furthermore, the sensitivity of creep life and creep damage predictions to the multi-axial parameter (α) is another limitation (Hyde et al., 2010c). Besides, stress-based damage models do not usually consider the effects of creep ductility on creep fracture behaviour in damage susceptible steels such as CSEF steels. Therefore, to overcome these limitations and capture the effect of creep ductility on creep damage of steels at high temperature, creep damage evolution is defined using an alternative approach, known as ductility exhaustion. In this

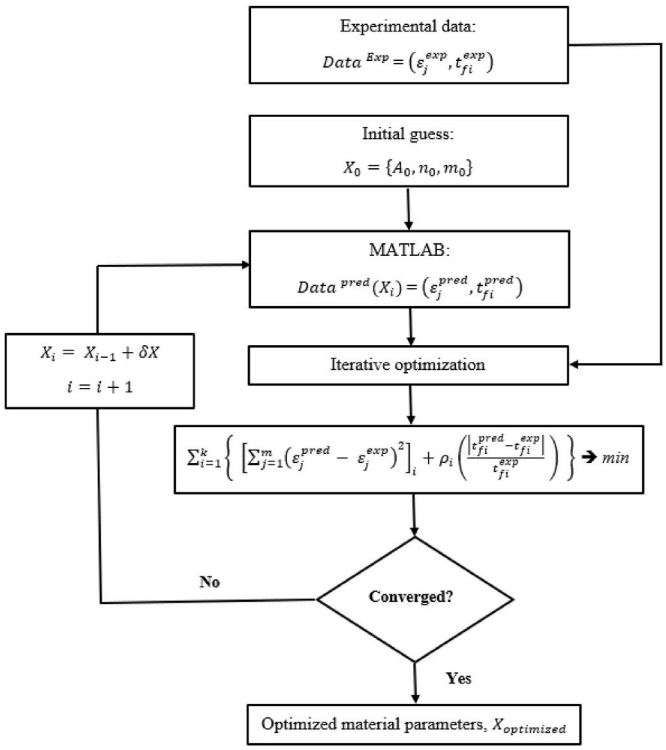

Fig. 6. Optimization flow chart used for obtaining the P91 base metal and simulated HAZ properties.

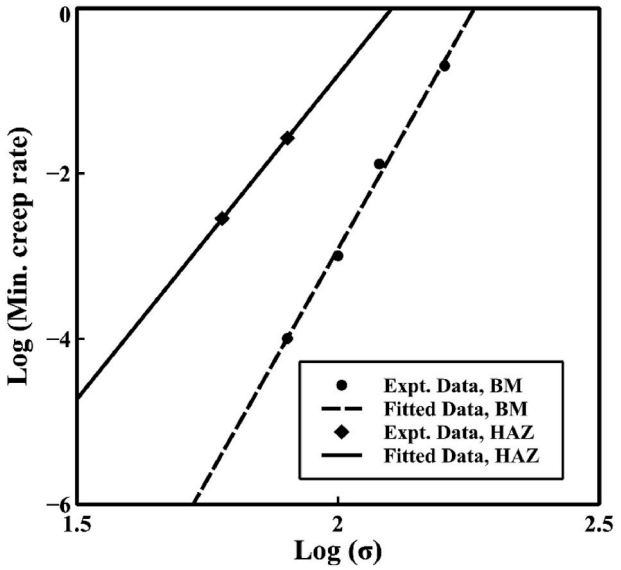

Fig. 7. Variation of the minimum creep strain rate with the stress, both on logarithmic scales, for the P91 BM and HAZ at 625 °C.

Table 3
Optimized material constants for the proposed strain-based damage model obtained for the P91 BM, WM and HAZ at 625 °C (stresses in MPa and times in hours).

	A	*n*	*m*
BM	5.88×10^{-26}	10.14	1.0×10^{-4}
HAZ	2.26×10^{-14}	5.23	4.56×10^{-5}
WM	3.0×10^{-27}	9.3	4.0×10^{-5}

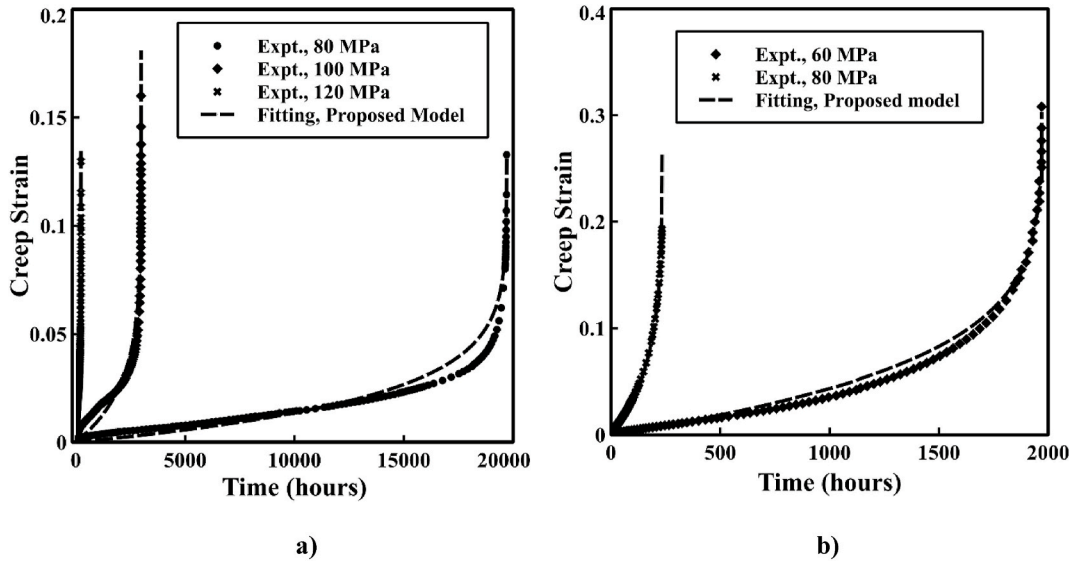

Fig. 8. Experimental and predicted uniaxial creep curves using the proposed strain-based model at 625 °C for: a) the P91 BM, and b) the P91 simulated HAZ.

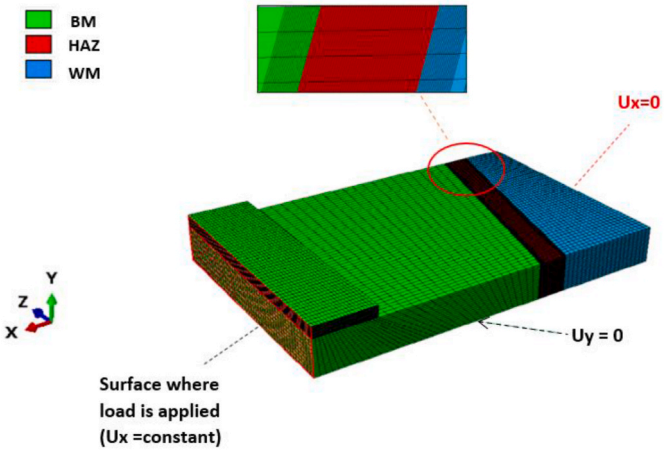

Fig. 9. The FE model of the CW creep test specimen showing the mesh, loading and boundary conditions.

approach, it is assumed that failure at a given material point occurs when the locally accumulated creep strain reaches its critical value (i.e. creep ductility of the material). Thus, the damage rate can be defined as follow:

$$\frac{d\omega}{dt} = \frac{\dot{\varepsilon}^c}{\varepsilon_f^*} \tag{4}$$

where $\dot{\varepsilon}^c$ *and* ε_f^* are the effective creep rate and multiaxial creep ductility, respectively. The multi-axial creep ductility can be computed using void growth models introduced in Section 3.2.

Based on Equations (1) and (4), the framework of our strain-based model can be established for a multi-axial stress state.

Under uniaxial loading conditions, the following relations can be obtained:

$$\sigma_1 = \sigma_{eq} = \sigma \tag{5}$$

The deviatoric stress can be generally expressed in the following tensorial form:

$$S_{ij} = \sigma_{ij} - \frac{\delta_{ij}\sigma_{kk}}{3} \tag{6}$$

where, δ_{ij} is the Kronecker delta function.

Under a uniaxial stress state, the stress component, σ_{kk}, can be expressed as:

$$\sigma_{kk} = \sigma_1 \tag{7}$$

Substituting Equation (7) into Equation (6) leads to the following expression:

$$S_{11} = \frac{2}{3}\sigma \tag{8}$$

where, σ and S_{11} are the applied stress and deviatoric stress component, respectively.

Hence, Equation (1) can be written as:

$$\frac{d\varepsilon^c}{dt} = A\left(\frac{\sigma}{1-\omega}\right)^n t^m \tag{9}$$

For a uniaxial stress state, the ratio of the multiaxial ductility to uniaxial ductility is given by:

$$\frac{\varepsilon_f^*}{\varepsilon_f} = 1 \tag{10}$$

Hence, the damage evolution in Equation (4) can be defined as follow:

$$\frac{d\omega}{dt} = \frac{\dot{\varepsilon}^c}{\varepsilon_f} \tag{11}$$

For a given material, stress and temperature conditions, creep ductility can be regarded constant value. By integrating Equation (11) with respect to time and substituting in Equation (9) for the damage parameter (ω), we can get an expression for the uniaxial creep strain rate in terms of creep ductility as follow:

$$\frac{d\varepsilon^c}{dt} = A\left(\frac{\varepsilon_f\,\sigma}{\varepsilon_f - \varepsilon^c}\right)^n t^m \tag{12}$$

Equation (12) represents an ordinary differential Equation with an initial condition (at t = 0, creep strain = 0). The solution of this equation yields an expression for the uniaxial (nominal) creep strain in terms of time, stress, and creep ductility as follow:

$$\varepsilon^c = \varepsilon_f - \left[\frac{-A\varepsilon_f{}^n(n+1)\sigma^n t^{m+1}}{m+1} + \varepsilon_f{}^{n+1}\right]^{\frac{1}{n+1}} \tag{13}$$

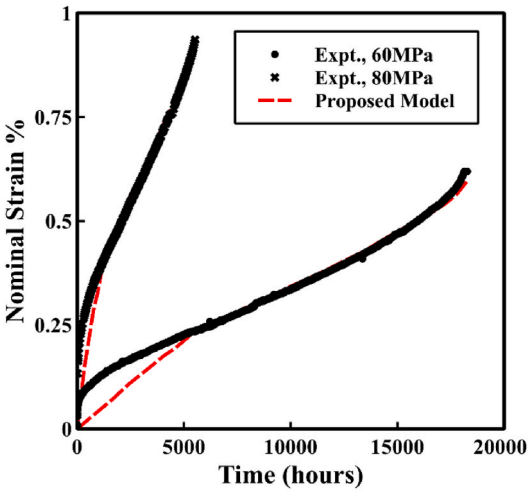

a

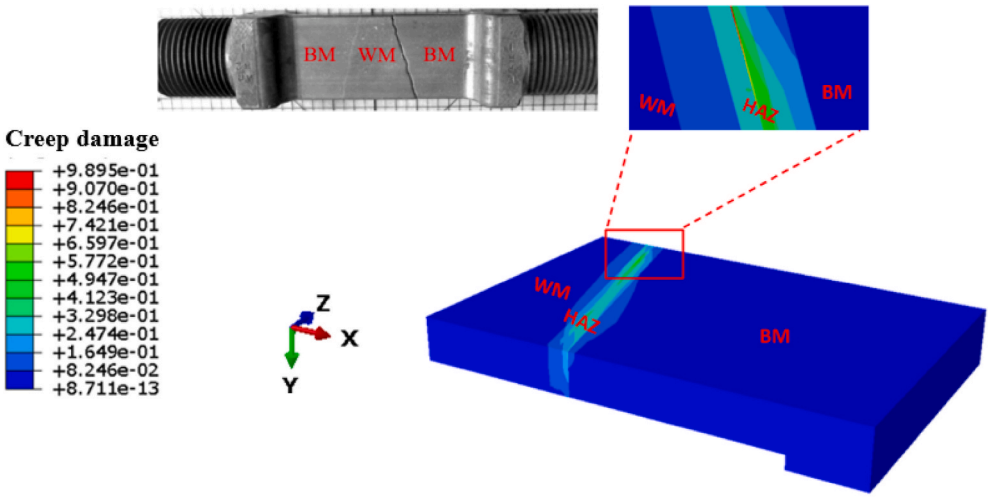

b

Fig. 10. a: Comparison of the predicted nominal creep strain curves with the experimental results of the P91 CW specimens at 625 °C. **b:** FE creep damage predictions for the CW specimen at a time close to failure at 80 MPa and 625 °C as compared to the experimentally observed failure mode.

As shown by Equation (13), the proposed strain-based model requires fewer material constants to be determined (A, n, m) as opposed to the stress-based Kachanov type CDM.

An expression for the creep failure time (under a uniaxial stress state) based on the modified model can be derived by assuming that at $t = t_f$ the local creep strain will reach the rupture ductility ε_f:

$$t_f = \left[\frac{\varepsilon_f\,(m+1)}{A\,(n+1)\,\sigma^n}\right]^{\frac{1}{m+1}} \tag{14}$$

Based on Equation (14), it is clear that creep failure life is influenced not only by the stress level but also by creep rupture ductility of the material. Thus, materials with poor creep ductility are likely to undergo premature failure. The link between creep ductility and creep damage or failure has also been experimentally observed for Grade 91 steels in previous investigations (Parker and Siefert, 2018; Siefert, 2019; Siefert et al., 2017).

It is worth noting that the effects of creep ductility on creep life of high-temperature steels cannot be directly captured from the conventional stress-based Kachanov-Rabotnov CDM, where creep life can be expressed as follow (for a uniaxial loading condition):

$$t_f = \left[\frac{(m+1)}{B(\varphi+1)\sigma^x}\right]^{\frac{1}{m+1}} \tag{15}$$

Therefore, the proposed strain-based model may offer improved life assessment as it allows the estimation of creep life for steels with variability in creep ductility. The capability of the model to provide insights into the effects of creep ductility on creep rupture lives of notched bars (under a net section stress of 100 MPa and temperature of 625 °C) is illustrated in Fig. 4. For a given stress level and temperature, variability in creep performance of CSEF steels with ductility can be observed. It is also evident that a linear correlation is present between creep rupture life and uniaxial creep ductility, with the creep rupture lives predicted to increase by 6x as the creep ductility increases from 5 to 25%.

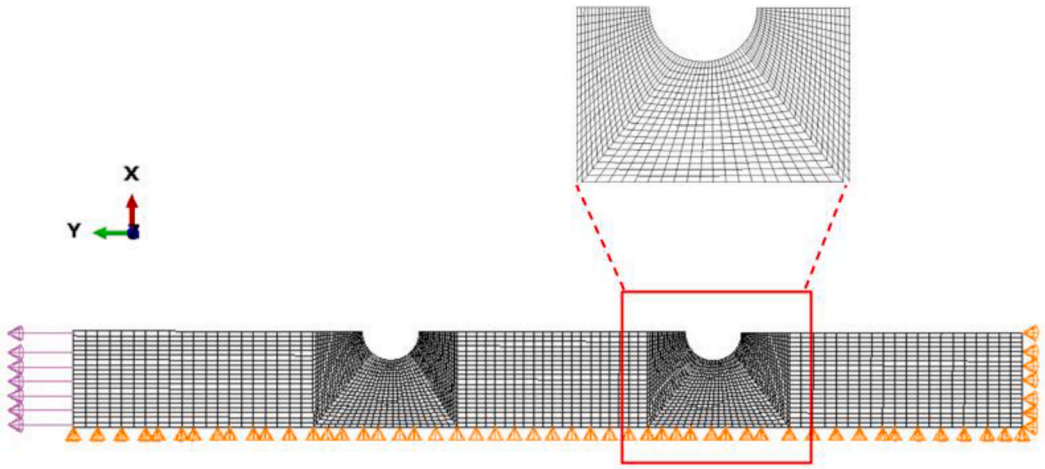

Fig. 11. The FE model of the double notched bar showing the mesh, loading and boundary conditions.

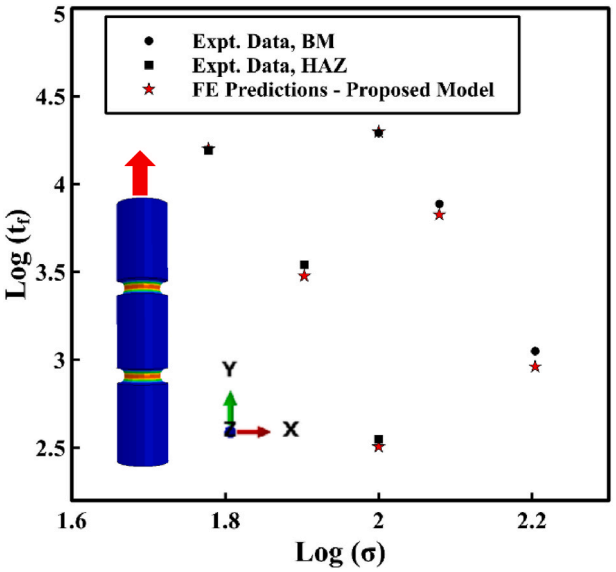

Fig. 12. Experimental and predicted notched bar creep rupture lives at 625 °C using the proposed strain-based model for the P91 BM and simulated HAZ (Net section stress in MPa and time in hours).

3.2. Constrained void growth models

Since components are typically operating under multi-axial stress state conditions, the multi-axial ductility (ε_f^*) should be computed when predicting creep damage and failure. Further, experimental studies have shown that creep ductility is influenced by stress states (Chang et al., 2015; Goyal and Laha, 2014; Goyal et al., 2014) and therefore the reduction in creep ductility under multiaxial stress state should be considered. The mathematical expressions which correlate the multi-axial ductility to the uniaxial ductility are often referred to as void growth models since they are developed on the basis of cavity growth mechanism under multiaxial stress states (Cocks and Ashby, 1980; Wen and Tu, 2014; Rice and Tracey, 1968). In the literature, several models have been proposed to evaluate the multiaxial ductility based on the uniaxial ductility, e.g., Rice and Tracey model (Rice and Tracey, 1968), Cocks and Ashby model (Cocks and Ashby, 1980), Wen and Tu model (Wen and Tu, 2014). These models typically express the ratio of the multiaxial ductility to uniaxial ductility in terms of the stress triaxiality ratio (hydrostatic stress/effective stress) as shown below (Equations 16–18):

Rice and Tracey model:

$$\frac{\varepsilon_f^*}{\varepsilon_f} = exp\left(\frac{1}{2} - \frac{3\sigma_m}{2\sigma_e}\right) \tag{16}$$

Cocks and Ashby model:

$$\frac{\varepsilon_f^*}{\varepsilon_f} = \frac{sinh\left[\frac{2}{3}\left(\frac{n-0.5}{n+0.5}\right)\right]}{sinh\left[2\left(\frac{n-0.5}{n+0.5}\right)\frac{\sigma_m}{\sigma_e}\right]} \tag{17}$$

Wen and Tu model:

$$\frac{\varepsilon_f^*}{\varepsilon_f} = \frac{exp\left[\frac{2}{3}\left(\frac{n-0.5}{n+0.5}\right)\right]}{exp\left[2\left(\frac{n-0.5}{n+0.5}\right)\frac{\sigma_m}{\sigma_e}\right]} \tag{18}$$

where σ_m and n are the hydrostatic (mean) stress and the steady state creep exponent, respectively.

Equations 16–18 are represented graphically in Fig. 5. A creep exponent (n = 10.14) is adopted in the Cocks-Ashby model and Wen-Tu model to compute the multi-axial creep ductility. The value of the stress triaxiality $\left(\frac{\sigma_m}{\sigma_e}\right)$ in the notched bar specimen is obtained at the skeletal point. At this point, the stress value is invariant with the creep exponent, n (Yatomi et al., 2004; Webster and Nikbin, 2003). As shown, there is a decreasing trend in the normalised creep ductility $\left(\frac{\varepsilon_f^*}{\varepsilon_f}\right)$ with the increase in stress triaxiality ratios $\left(\frac{\sigma_m}{\sigma_e}\right)$. By comparing the experimental data of plain and notched bar tests of Grade 91 BM to the theoretical predictions, it is evident that the Cocks-Ashby and Wen-Tu models give better fit. However, the Cocks-Ashby model gives infinite ductility values at low degrees of constraint (not realistic) because of the *sinh* term. It may be pointed that the Wen-Tu model may slightly overestimate the multi-axial creep ductility in the range $0.33 < \frac{\sigma_m}{\sigma_e} < 1.5$. However, as the degree of stress triaxiality increases, it is expected that both the Cocks-Ashby model and Wen-Tu would give similar results. In this study, the exponential law proposed by Wen and Tu (Equation (18)) will be used to predict the multi-axial ductility at various degrees of constraint based on the experimental uniaxial creep ductility. The uniaxial creep ductility (ε_f) at a given temperature can be estimated as the average value of the uniaxial creep rupture strains at different stresses (Zhang et al., 2017; Oh et al., 2011; Kim et al., 2013; Zhang et al., 2020a).

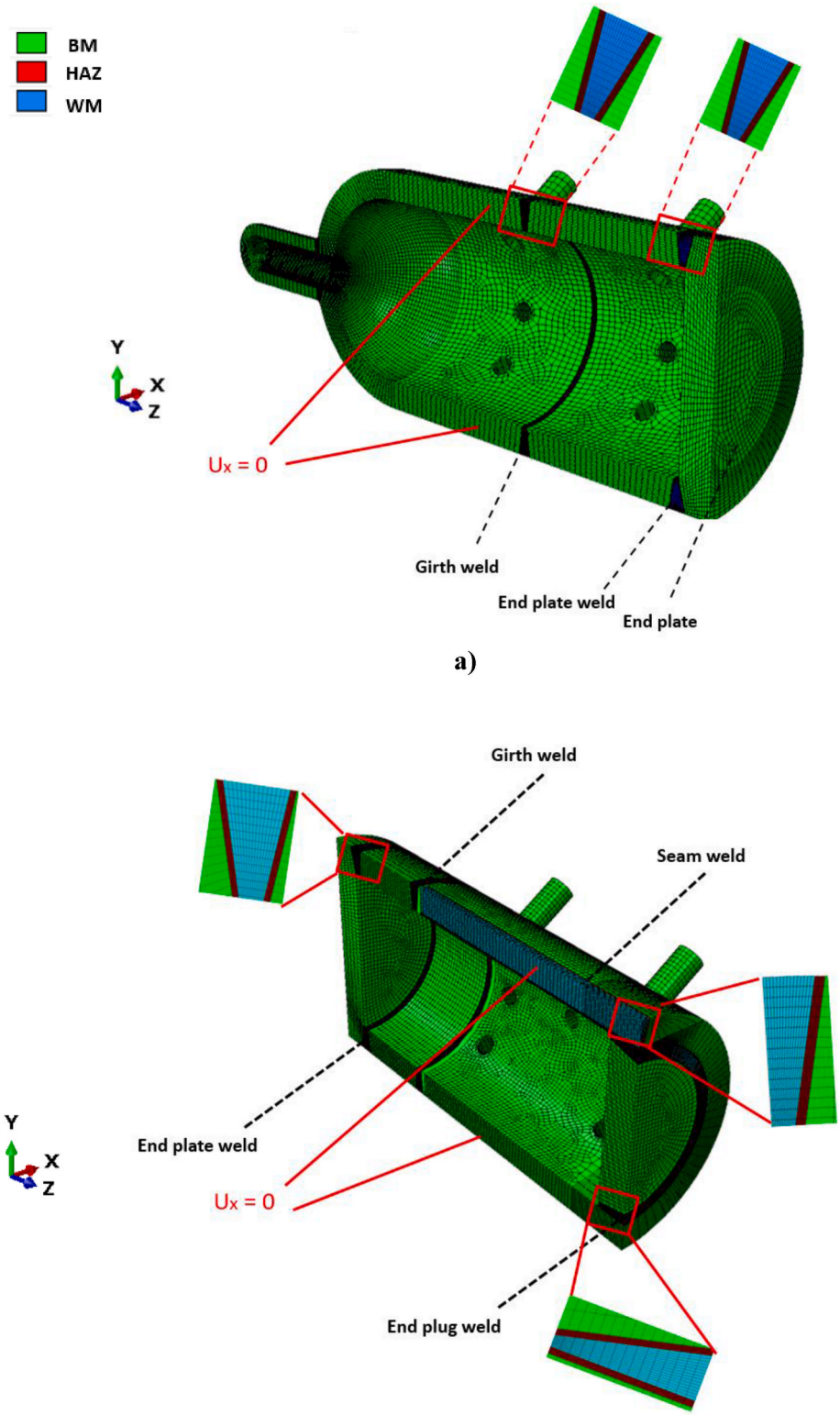

Fig. 13. The FE model (mesh scheme & boundary conditions) of a) Vessel-1, and b) Vessel-2.

4. Determination of material properties

The constitutive model presented in the previous section requires material constants to be derived. Thus, in this section we demonstrate the optimization procedure followed to determine the material parameters of the proposed damage model for each weld constituent (BM, WM, HAZ) based on accelerated creep tests in conjunction with the FE simulation. Identification of the BM and HAZ creep properties is detailed in Section 4.1, while the approach adopted in obtaining the WM creep properties is outlined in Section 4.2.

4.1. BM and HAZ properties

An optimization code is developed in MATLAB to determine creep

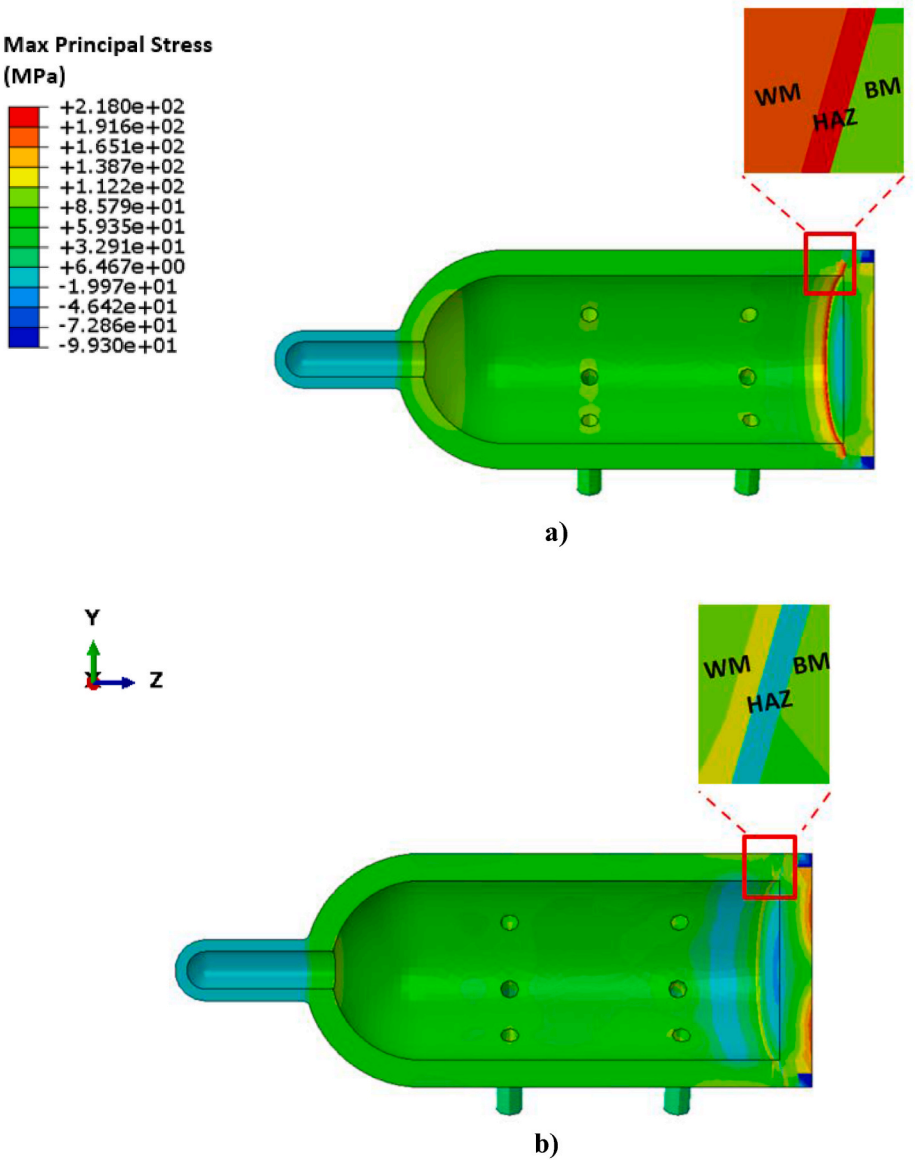

Fig. 14. Distribution of the maximum principal stress in Vessel-1 at: a) Just before crack initiation, and b) at failure. (NB: The magnified section taken through the wall thickness indicates the distribution of the max. principal stress in the endplate weldment).

properties for both the P91 BM and simulated HAZ by fitting a group of experimental creep curves to the uniaxial creep strain curves using Equation (13). The optimization flow chart is depicted in Fig. 6, with the objective function taking the following form:

$$\sum_{i=1}^{k}\left\{\left[\sum_{j=1}^{m}\left(\varepsilon_j^{pred}-\varepsilon_j^{exp}\right)^2\right]_i+\rho_i\left(\frac{\left|t_{fi}^{pred}-t_{fi}^{exp}\right|}{t_{fi}^{exp}}\right)\right\}\rightarrow \min \tag{19}$$

where k denotes the number of creep curves corresponding to different stress levels; m the number of points per curve; ρ_i a scaling factor accounting for the time error in the optimization process and its value ranges from 0 to 1 (its value can be obtained by minimizing equation (19)); superscript *pred* denotes the quantities from predictions and superscript *exp* denotes the quantities measured from experiments.

The optimization process requires initial values for the material properties to be provided. Therefore, the relationship between the steady-state creep rate and the applied stress for the P91 plain bars, shown in Fig. 7, is utilized for this purpose. Material properties obtained from the optimization are listed in Table 3 and the predicted uniaxial creep curves for both the base metal and simulated HAZ are shown in Fig. 8. It should be noted that the uniaxial creep ductility of the BM and simulated HAZ are determined from the uniaxial creep tests on plain bars as the average creep rupture strains. Uniaxial creep ductility values of the BM and simulated HAZ were calculated as 0.17 and 0.25, respectively.

4.2. Weld metal properties

The creep properties of the WM are determined using an inverse approach where the FE predictions of CW creep responses are compared with the experimental results of the CW creep tests (Ragab et al., 2021). Initial material properties were first assigned to the weld metal. Following a series of FE analyses with the known properties for the BM and HAZ, the optimized weld metal creep properties are achieved by minimizing the difference between the FE predictions and the experimental data of the cross-weld creep tests. The FE damage analysis has been conducted on the CW (BM, WM, HAZ) at 625 °C using the strain-based damage model, given by Equations (1), (4) and (18), in conjunction with the base metal and HAZ properties listed in Table 3. 3D quadratic continuum elements with reduced integrations (C3D20R) are

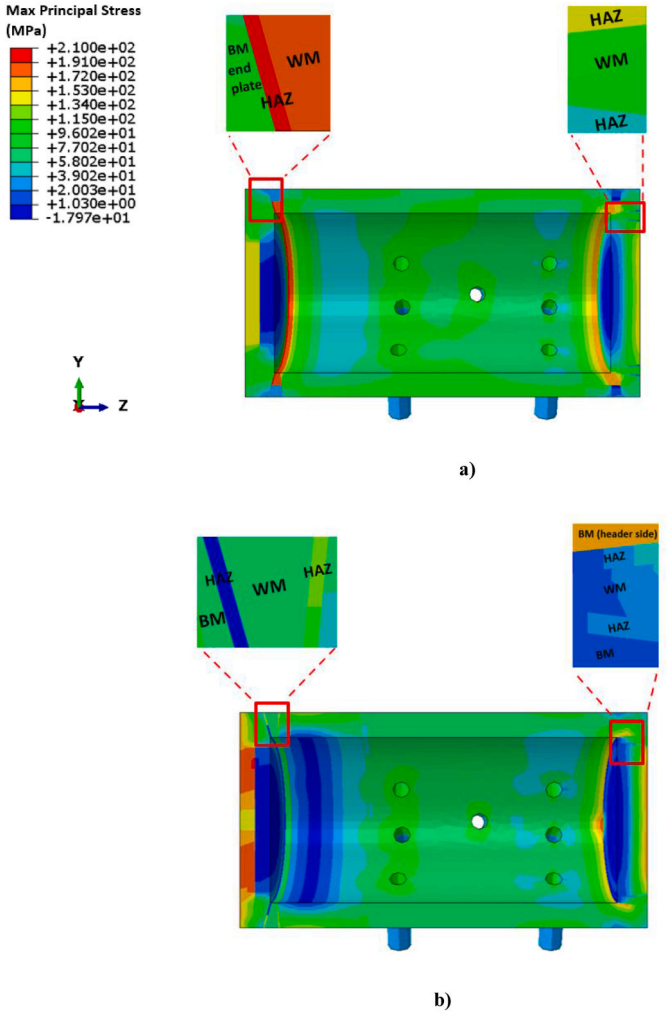

Fig. 15. Distribution of the maximum principal stress in Vessel-2 at: a) Just before crack initiation, and b) at failure. (NB: The magnified sections taken through the wall thickness indicate the distribution of the max. principal stress in the endplate and end plug weldment).

used to model the CW specimen in ABAQUS (ABAQUS 2019 online documentation, 2019). Due to the symmetry of the problem, only a quarter of the geometry was modelled, using plane symmetry boundary conditions as shown in Fig. 9. The mesh assigned for the CW specimen is illustrated in Fig. 9, with a local mesh refinement applied at the weld interface regions where stresses change rapidly. Based on a prior mesh convergence study, a total of 28,000 elements are used to model the geometry, resulting in negligible stress variations relative to the chosen mesh. Creep properties obtained for the WM are shown in Table 3. Uniaxial creep ductility of the WM is determined inversely from the FE analysis of the CW as 0.17. In the FE damage analysis, material failure at a point is assumed to occur when the damage variable (ω) approaches unity, and therefore, creep crack initiation is defined as the first element reaching a damage level ($\omega \approx 1$). To simulate time-dependent creep damage accumulation, a user defined subroutine is implemented in ABAQUS to reduce the element stiffness.

The nominal strain *vs* time curves for the CW specimens are calculated by dividing the gauge length elongation at a given time by the initial gauge length. The predicted creep curves at a stress of 60 MPa and 80 MPa are compared against the experimental results, as illustrated in Fig. 10a. Further, creep damage is predicted for the CW specimen subjected to an 80 MPa stress, as depicted in Fig. 10b, which shows significant creep damage in the HAZ region compared with the BM and WM. Creep failure is predicted to occur in the HAZ for both CW specimens tested under 60 MPa and 80 MPa, which is in agreement with the experimental results reported in Table 2.

5. Capabilities of the proposed model

In this section, the capability of the proposed modelling approach to predict creep damage and failure will be examined under bi-axial stress states using notched bars (Section 5.1) and under complex multi-axial stress state conditions using Grade 91 pressurized welded vessels (Section 5.2). It should be noted that the experimental data used for comparison are not used in the identification of material parameters presented in Section 4.

5.1. FE creep damage modelling of notched bars

A FE creep damage analysis has been performed on the P91 notched bars through the implementation of the proposed strain-based model to predict creep rupture lives in notched bars at 625 °C. To simulate creep damage and failure in the notched bars, a similar technique as that illustrated in Section 4.2 is implemented, i.e., a user defined subroutine is utilized to reduce the element stiffness and to calculate critical damage progression. The FE predictions are compared against the experimental results for the P91 base metal (BM) and simulated HAZ to examine the accuracy of the damage model in predicting creep lives under biaxial stress states. The FE model of the notched bar is shown in Fig. 11. The notched bar is modelled using axisymmetric elements with reduced integrations (CAX8R) in ABAQUS. Based on the mesh convergence study, a total of 3600 elements are used in the model, resulting in insignificant stress variations relative to the chosen mesh. Finer mesh has been assigned near the notches, where stresses vary rapidly. Fig. 12 compares the numerical predictions of creep rupture lives of the notched bars based on the proposed model with the experimental results. In Fig. 12, creep rupture lives are plotted against the net section mean axial stress. As shown, the proposed model satisfactorily predicts the experimental results of notched bar creep tests.

5.2. Creep damage modelling of the vessel tests

This section illustrates the implementation of the proposed damage evolution model in the FE software ABAQUS to simulate the long-term creep tests on Grade 91 vessels introduced earlier in Section 2.2 and shown in Figs. 2 and 3. First, the finite element models of the vessels are presented in Section 5.2.1. Then, the results related to the stress and damage analysis are presented and discussed in Section 5.2.2. Besides, the accuracy of the model in predicting creep damage, creep crack growth and failure is assessed by comparing the FE predictions of the simulated vessels to the corresponding experimental data, as detailed in Section 5.2.3.

5.2.1. FE model of the Grade 91 vessels

A FE continuum damage-based analysis is carried out on two Grade 91 vessel components at an average temperate of 625 °C and internal pressure of 15 MPa in the commercial FE software ABAQUS (ABAQUS 2019 online documentation, 2019). The layout and dimensions of these structures are as illustrated in Figs. 2 and 3. The ductility-based model as given by Equations (1), (4) and (18) is embedded into a user defined subroutine in ABAQUS to characterise the mechanical behaviour of the vessels and the associated weldment under high-temperature creep conditions. The weld regions in both vessels are assumed to comprise three material phases: BM, WM and HAZ as shown in Fig. 13a and Fig. 13b, with the corresponding creep damage properties as listed in Table 3. Both vessels are modelled using 3D linear continuum elements with reduced integrations (C3D8R). The mesh schemes for both vessels are shown in Fig. 13a and b, with a local mesh refinement assigned to the weld interface regions where material discontinuity exists. In total, vessel-1 is modelled with 170,000 elements, while vessel-2 mesh

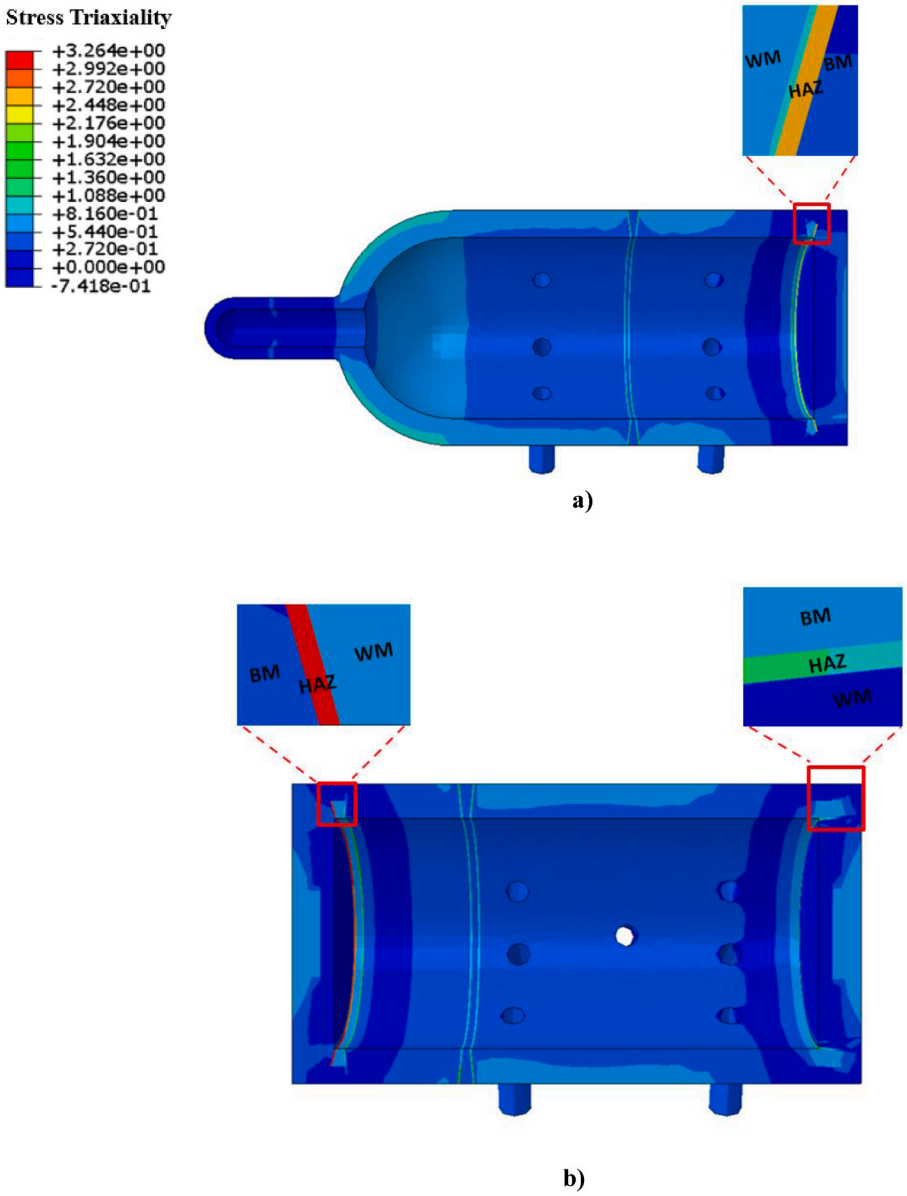

Fig. 16. Stress triaxiality distributions before creep crack initiation in a) Vessel-1, and b) Vessel-2.

comprises 200,000 elements. Taking an advantage of the problem symmetry, only half of the geometry was modelled, using plane symmetry boundary conditions as illustrated in Fig. 13a and b. In both vessels, an internal pressure of 15 MPa was applied to the inner surfaces of the main pipes and the stubs, while a proportion of this pressure was applied as an axial thrust to the ends of the vessels and stub tubes. Rigid body motions are prevented in both vessels and the axial displacements at the end of stub tubes are maintained constant. In the FE damage analysis, the effects of residual stresses and any secondary loads, e.g., systems loads induced by manufacturing or hanger bending etc, are neglected.

5.2.2. *General stress and damage analysis*

The ductility-based damage evolution model as defined by Equations (1), (4) and (18) is implemented into user-defined subroutines in the FE software ABAQUS to determine the time-dependent creep behaviour and the accumulation of creep damage. In the ductility exhaustion approach, material failure at a given point is assumed to occur when the local strain reaches creep rupture ductility of the material, at which point the damage variable (ω) approaches unity. The uniaxial creep ductility employed in Equation (4) is estimated based on accelerated uniaxial tensile creep tests as the average value of the uniaxial creep rupture strains at different stresses. In the work presented by Zhang et al., 2017, 2020a on 9Cr–1Mo steels at 600 °C and under different stress conditions, the average creep rupture strain was found to yield a reasonable approximation of material creep ductility. Further, a constant creep ductility value at a given temperature is assumed in the work by Wen and Tu (2014) since the local stress in the vicinity of the crack tip remains high. However, creep ductility may change with stresses (Wen et al., 2016; Goyal and Laha, 2014) and hence the long-term creep rupture ductility should ideally be obtained from long-term creep tests. The availability of such tests is currently limited.

The predicted maximum principal stress distributions at different creep times in Vessel-1 and Vessel-2 are shown in Fig. 14 and Fig. 15, respectively. At longer term, the influence of the maximum principal stress on creep damage and rupture becomes more pronounced (Goyal et al., 2014). In Vessel-1, shown in Fig. 14a, a high stress concentration is predicted across the endplate weld in the HAZ region prior to crack initiation. It is worth noting that in Vessel-1, stress distributions at the domed end fitting are relatively lower than those predicted at the flat

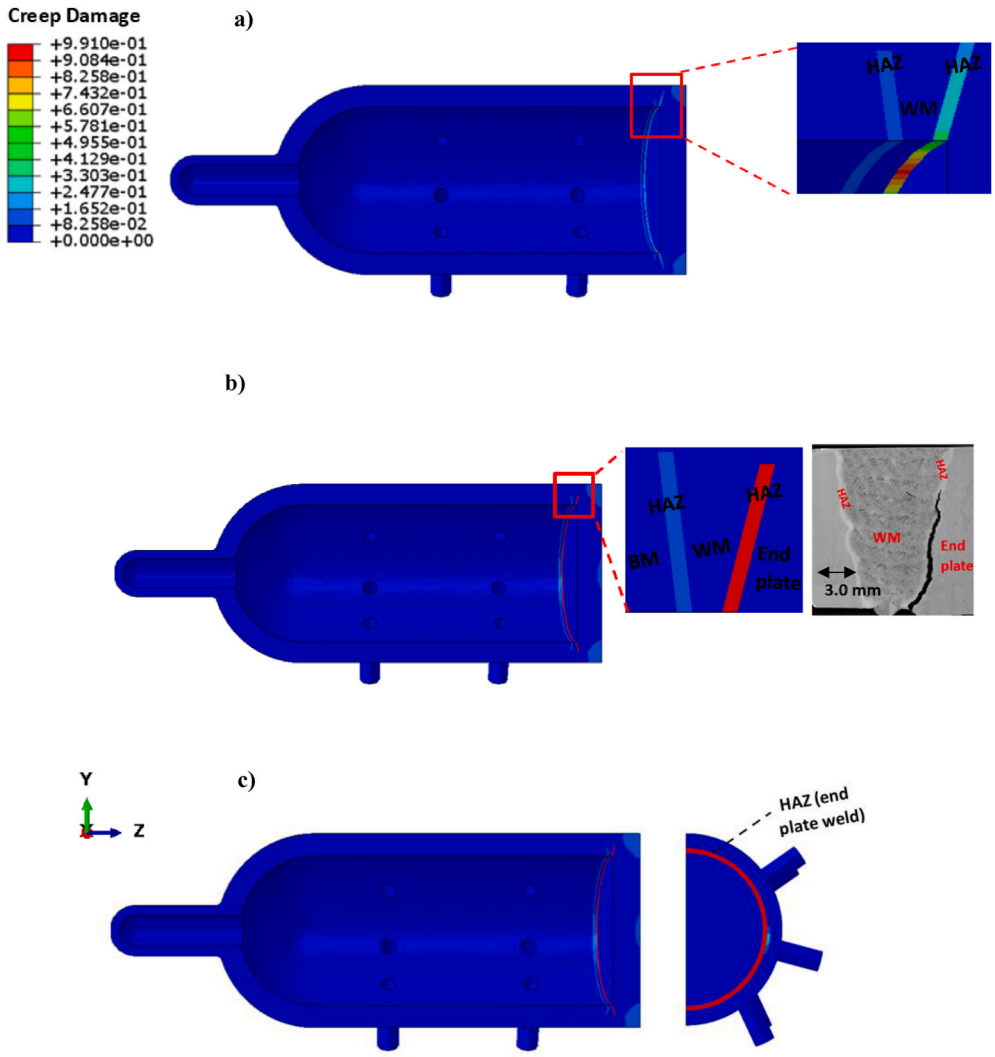

Fig. 17. Predicted creep damage distribution and cracking in Vessel-1 at: a) 8800 h, b) at failure (the magnified sections on the right compare the predicted through-wall cracking in the HAZ of the end plate weld to the corresponding experimental observations), and c) predicted circumferential cracking in the HAZ of the end plate weld.

end cap, as shown in Fig. 14a, which indicates that the domed end cap geometry provides better creep performance for minimizing stress concentrations. Similarly, the FE predictions for Vessel-2 test show that the maximum principal stress tends to peak in the HAZ of the endplate weld and end plug weld regions before crack starts to initiate with higher stresses predicted in the endplate weld than in the weld associated with the end plug, as illustrated in Fig. 15a. The predicted maximum stresses at a time close to failure are plotted in Figs. 14b and 15b, which show that stress offloading may have occurred during creep process in the HAZ of the endplate and end plug weldment, indicating creep damage in these regions. In addition to the local stresses, the stress triaxiality parameter $\left(\frac{\sigma_m}{\sigma_e}\right)$ is obtained for Vessel-1 and Vessel-2 before crack initiation, as shown in Fig. 16a and Fig. 16b, respectively. Evidently, a highly localised triaxial stress state can be observed in the HAZ of the weldment associated with the end closures (i.e., end plug and endplate weldment). These results emphasise that the triaxiality parameter plays a key role in the multi-axial creep ductility and damage behaviour. This agrees with the findings reported by (Zhang et al., 2020b).

5.2.3. Creep damage and crack growth in weldment

Creep crack growth analysis is also undertaken on the basis of the proposed ductility exhaustion model. Creep crack initiation can be defined as the first element reaching a damage variable $\omega \approx 1$ at the integration point (Hyde et al., 2001; Ragab et al., 2021). To simulate creep crack growth, a user subroutine is developed in ABAQUS to reduce the element stiffness to nearly zero after the element has failed. Hence, creep crack growth in this work has been simulated as the accumulation of the damaged elements zone. Fig. 17 and Fig. 18 respectively show the predicted creep damage patterns at 625 °C for Vessel-1 and Vessel-2 at different creep time intervals. The FE damage analysis results of Vessel-1 indicate that crack initiation is predicted to occur in the HAZ of the end plate weld at about 8800 h (this is the region where high stress concentrations are predicted), as shown in Fig. 17a. Following crack initiation, cracking in the HAZ within the end plate weldment is found to connect to the inside surface of the vessel and extend to >70% wall thickness, as shown in Fig. 17b. The predicted through-wall cracking as well as the circumferential cracking associated with the end plate weld at failure are shown in Fig. 17b and c. As shown, the predicted creep damage/crack locations using the proposed model are in good agreements with the experimental observations reported by (Parker and Siefert, 2020). It can also be seen that while the HAZ on the end plate side of the weld has developed creep damage/cracking, the HAZ on the other side of the weld has developed no cracking, which is consistent with the experimental observations shown in Fig. 17b. Further, creep

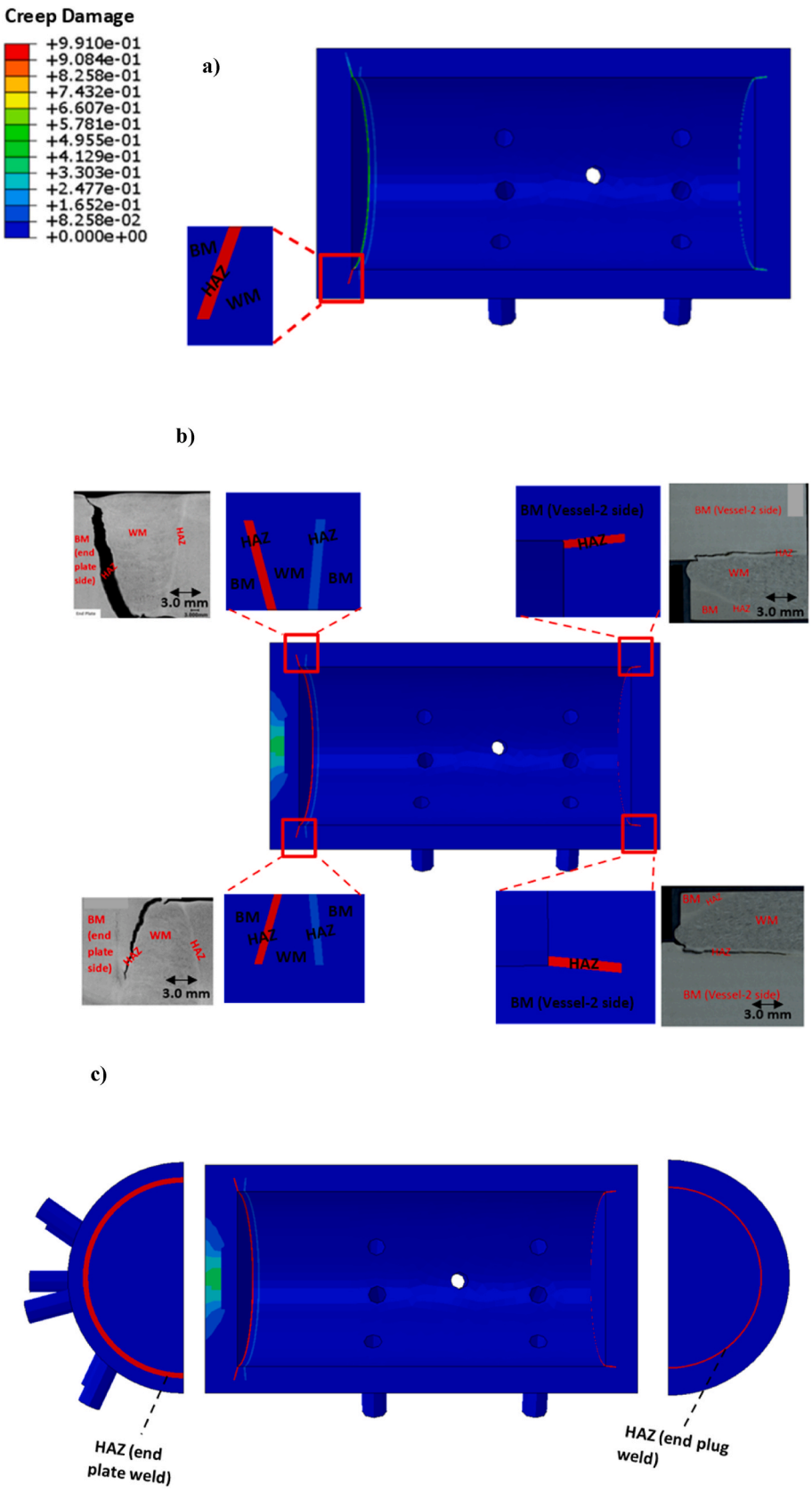

Fig. 18. Predicted creep damage distribution and cracking in Vessel-2 at: a) 6500 h, b) at failure (the magnified sections on the right compare the predicted through-wall cracking in the HAZ of the end plug weld to the experimental results while those on the left compare the predicted through-wall crack in the HAZ of the end plate weld to the corresponding experimental data), and c) predicted circumferential cracking in the HAZ of the end plate weld (left) and end plug weld (right). (Experimental results are adapted from ref (Parker and Siefert, 2020)).

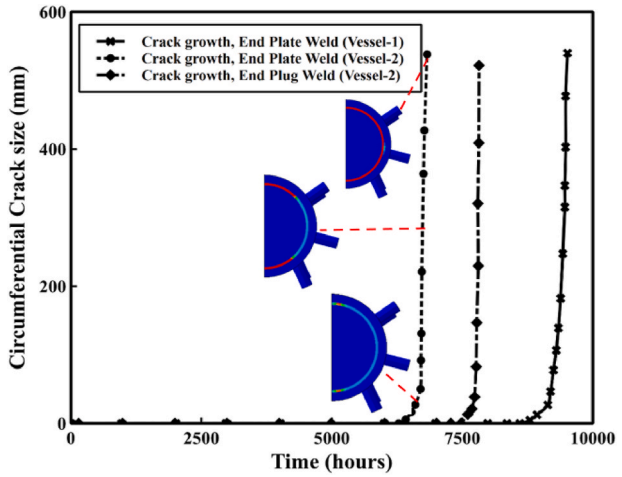

Fig. 19. FE predictions of circumferential creep crack growth along the inside surface of the end fittings weldment of Vessel-1 and Vessel-2.

rupture life of Vessel-1 is predicted at about 9515 h, which is corresponding well with the experimental failure life of 10,000 h. With regard to Vessel-2, crack initiation is predicted in the HAZ on the end plate side of the weld after about 6500 h of creep time, as shown in Fig. 18a. The stress analysis performed earlier has revealed high stresses in this region, as shown in Fig. 15a. Following crack initiation in Vessel-2, creep crack on the end plate weld is found to propagate in a similar manner to that predicted earlier for Vessel-1 (i.e. cracking in the HAZ on the end plate side of the weld connects to the inside diameter of the vessel and extends to >70% wall thickness). After about 6800 h, the end plate weld is predicted to fail and the locations of the through-wall cracking and the circumferential crack along the HAZ of the end plate weld are as shown in Fig. 18b and c. The cracking patterns obtained by the proposed model correlate reasonably well with the experimental results shown in Fig. 18b. The simulation has continued, and crack initiation is predicted after 7450 h in the HAZ on the end plug weld. After about 7820 h, a fully circumferential cracking is predicted in the HAZ associated with the end plug weld, as shown in Fig. 18c. Further, cracking is found to extend through the wall thickness as shown in Fig. 18b, which is in a good agreement with the corresponding experimental results presented in Fig. 18b. At this location, it is evident that only the HAZ on the header side of the end plug weld has developed cracking due to the higher bending stresses there. Based on the FE damage analysis, no damage/cracking has been detected for the girth weld or the seam weld (in agreement with the experimental observations related to vessels testing (Parker and Siefert, 2020)).

Creep crack growth for Vessel-1 and Vessel-2 weldment are predicted based on the proposed CDM and the results are depicted in Fig. 19. The successive positions of the crack surface growth on the end plate weldment of Vessel-2 at different creep times are also shown in Fig. 19. As shown, crack initiates in the end plate and end plug weldment after 90–95% of creep life had been consumed. It can also be seen that, following crack initiation, cracking in the weld starts to propagate rapidly until creep failure, where the critical crack length is reached. As presented in Fig. 19, the end plate weld of Vessel-2 is predicted to fail first, followed by the end plug weld. In summary, creep rupture lives of Vessel-1 and Vessel-2 as predicted by the proposed model are found in good agreement with the corresponding experimental results of vessels tests.

6. Conclusion and future work

In this study, a modified ductility based CDM model was developed and used to model the creep crack growth in welded pressurized vessels. The proposed model not only demonstrated good predictive capabilities but was also able to interpret some of the experimental findings related to the damage and cracking in the vessel tests, facilitating an improved understanding into Type IV failure in Grade 91 steel welded structures. The key conclusions are:

- The predicted creep rupture lives of the notched bars based on the proposed CDM model were in good agreement with the experimental creep failure lives.
- Creep damage/cracking in simulated vessels was predicted to occur in the HAZ of the weldment associated with the end fittings (i.e., end plug and endplate weldment), which is in good agreement with the experimental results of vessels tests. Moreover, the predicted creep rupture lives of the vessels by the proposed model showed good correlation with the corresponding experimental creep lives.
- The highly localised stresses and stress triaxialities in the HAZ region were found to play a key role in the occurrence of Type IV failure in the vessel weldment. This is possibly assisted by the enhanced bending due to the geometry of the end closures.

Following are brief insights into future work:

- At longer term the multiaxial creep ductility may change, possibly due to voids coalescence and micro-cracks formation (Wen et al., 2016). This will be explored in the future work through experimental testing and numerical modelling. Since the multi-axial ductility is stress state and stress level dependent, the current creep ductility-based model will be further improved in future work to consider more accurately the variability in the multiaxial behaviour.
- CSEF steel weldment is metallurgically complex. Therefore, the current methodology adopted to obtain creep properties of the weldment could be improved in future work through utilizing miniature specimen testing (Wen et al., 2019) and local hardness mapping to characterise the microstructural gradient in the HAZ and hence derive more accurate properties.
- The large level of scatter typically observed in creep data may constitute a challenge towards the implementation of the proposed model for real life applications. This could be alleviated by employing statistical approaches to consider the variability in material properties, and therefore, obtain more reliable creep life predictions.

Credit author statement

Raheeg Ragab: Conceptualization, Methodology, Software, Formal analysis, Investigation, Data curation, Writing – original draft. **Jonathan Parker:** Conceptualization, Methodology, Writing – review & editing, Supervision. **Ming Li:** Conceptualization, Methodology, Writing – review & editing, Supervision. **Tao Liu:** Conceptualization, Methodology, Writing – review & editing, Supervision, Project administration, Funding acquisition. **Wei Sun:** Conceptualization, Methodology, Writing – review & editing, Supervision, Project administration, Funding acquisition.

Declaration of competing interest

The authors declare that they have no known competing financial interests or personal relationships that could have appeared to influence the work reported in this paper.

Acknowledgments

This work was supported by the Engineering and Physical Sciences Research Council (EPSRC). The funding is provided through the EPSRC Centre for Doctoral Training in Resilient Decarbonised Fuel Energy Systems (Grant number: EP/S022996/1). The work was also partly sponsored by the Biomass and Fossil Fuel Research Alliance (BF2RA).

The authors would also like to acknowledge EPRI for permission to use their experimental results and publish this paper.

References

ABAQUS 2019 online documentation, 2019. © Dassault Systèmes.

Alang, N., Nikbin, K., 2018. An analytical and numerical approach to multiscale ductility constraint based model to predict uniaxial/multiaxial creep rupture and cracking rates. Int. J. Mech. Sci. 135, 342–352. https://doi.org/10.1016/j.ijmecsci.2017.11.030.

Chang, Y., Xu, H., Ni, Y., Lan, X., Li, H., 2015. The effect of multiaxial stress state on creep behavior and fracture mechanism of P92 steel. Mater. Sci. Eng. A 636, 70–76. https://doi.org/10.1016/j.msea.2015.03.056.

Choudhary, B.K., Palaparti, D.P.R., 2012. Comparative tensile flow and work hardening behaviour of thin section and forged thick section 9Cr-1Mo ferritic steel in the framework of Voce equation and Kocks-Mecking approach. J. Nucl. Mater. 430, 72–81. https://doi.org/10.1016/j.jnucmat.2012.06.046.

Cocks, A.C.F., Ashby, M.F., 1980. Intergranular fracture during power-law creep under multiaxial stresses. Met. Sci. 14 (8–9), 395–402. https://doi.org/10.1179/030634580790441187.

Dyson, B., 2000. Use of CDM in materials modelling and component creep life prediction. J. Presssure Vessel Technol. 122, 281–296. https://doi.org/10.1115/1.556185.

Goyal, S., Laha, K., 2014. Creep life prediction of 9Cr–1Mo steel under multiaxial state of stress. Mater. Sci. Eng. A 615, 348–360. https://doi.org/10.1016/j.msea.2014.07.096.

Goyal, S., Laha, K., Das, C.R., Selvi, S.P., Mathew, M.D., 2013. Finite element analysis of uniaxial and multiaxial state of stress on creep rupture behaviour of 2.25Cr–1Mo steel. Mater. Sci. Eng. A 563, 68–77. https://doi.org/10.1016/j.msea.2012.11.038.

Goyal, S., Laha, K., Das, C.R., et al., 2014. Effect of constraint on creep behavior of 9Cr-1Mo steel. Metall. Mater. Trans. 45, 619–632. https://doi.org/10.1007/s11661-013-2025-z.

Hayhurst, D.R., Dimmer, P.R., Morrison, C.J., 1984. Development of continuum damage in the creep rupture of notched bars. Phil. Trans. R Soc. Lond. A 1984 311, 103–129.

Holdsworth, S., 2019. Creep-ductility of high temperature steels: a review. Metals 9 (3), 342. https://doi.org/10.3390/met9030342.

Hosseini, E., Holdsworth, S.R., Mazza, E., 2013. Stress regime-dependent creep constitutive model considerations in finite element continuum damage mechanics. Int. J. Damage Mech. 22, 1186–1205. https://doi.org/10.1177/1056789513479810.

Hyde, T.H., Sun, W., 2000. Determining high temperature properties of weld materials. JSME Int. J. of Solid Mechanics & Material Engineering, Series A 43, 408–414. https://doi.org/10.1299/jsmea.43.408.

Hyde, T.H., Sun, W., Becker, A.A., 2001. Creep crack growth in welds: a damage mechanics approach to predicting initiation and growth of circumferential cracks. Int. J. Pres. Ves. Pip. 78, 765–771. https://doi.org/10.1016/S0308-0161(01)00088-6.

Hyde, T.H., Sun, W., Becker, A.A., Williams, J.A., 2004. Creep properties and failure assessment of new and fully repaired P91 pipe welds at 923 K. Proc. Inst. Mech. Eng. Part L: J. Materials: Design and Applications 218, 211–222. https://doi.org/10.1177/146442070421800305.

Hyde, T.H., Becker, A.A., Sun, W., Williams, J.A., 2006. Finite element creep damage analyses of P91 pipes. Int. J. Pres. Ves. Pip. 83, 853–863. https://doi.org/10.1016/j.ijpvp.2006.08.013.

Hyde, C.J., Hyde, T.H., Sun, W., Becker, A.A., 2010a. Damage mechanics-based predictions of creep crack growth in 316 stainless steel. Eng. Fract. Mech. 77 (12), 2385–2402. https://doi.org/10.1016/j.engfracmech.2010.06.011.

Hyde, T.H., Saber, M., Sun, W., 2010b. Creep crack growth data and prediction for a P91 weld at 650 °C. Int. J. Pres. Ves. Pip. 87, 721–729. https://doi.org/10.1016/j.ijpvp.2010.09.002.

Hyde, T.H., Saber, M., Sun, W., 2010c. Testing and modelling of creep crack growth in compact tension specimens from a P91 weld at 650°C. Eng. Fract. Mech. 77 (15), 2946–2957. https://doi.org/10.1016/j.engfracmech.2010.03.043.

Kachanov, L., 1958. On rupture time under condition of creep. Izvestia Akademi Nauk USSR, Otd. Techn. Nauk, Moskwa 8, 26–31.

Kim, N.H., Oh, C.S., Kim, Y.J., Davies, C.M., Nikbin, K.M., Dean, D.W., 2013. Creep failure simulations of 316H at 550°C: Part II – effects of specimen geometry and loading mode. Eng. Fract. Mech. 105, 169–181. https://doi.org/10.1016/j.engfracmech.2013.04.001.

Li, M., Barrett, R.A., Scully, S., Harrison, N.M., Leen, S.B., O'Donoghue, P.E., 2016. Cyclic plasticity of welded P91 material for simple and complex power plant connections. Int. J. Fatig. 87, 391–404. https://doi.org/10.1016/j.ijfatigue.2016.02.005.

Liu, Y., Murakami, S., 1998. Damage localisation of conventional creep damage models and proposition of a new creep damage analysis. JSME Int. J. of Solid Mechanics & Material Engineering, Series A 41 (1), 57–65. https://doi.org/10.1299/jsmea.41.57.

Masuyama, F., 1999. New developments in steels for power generation boilers. In: Advanced Heat Resistant Steel for Power Generation. Institute of Materials, pp. 33–48.

Meng, Q., Wang, Z., 2019. Creep damage models and their applications for crack growth analysis in pipes: a review. Eng. Fract. Mech. 205, 547–576. https://doi.org/10.1016/j.engfracmech.2015.09.055.

Naumenko, K., Kostenko, Y., 2009. Structural analysis of a power plant component using a stress-range-dependent creep-damage constitutive model. Mater. Sci. Eng., A 510 (511), 169–174. https://doi.org/10.1016/j.msea.2008.04.096.

Nikbin, K., 2017. A unified multiscale ductility exhaustion-based approach to predict uniaxial, multiaxial creep rupture and crack growth. Eng. Fract. Mech. 179, 240–259. https://doi.org/10.1016/j.engfracmech.2017.04.046.

Nikbin, K.M., Smith, D.J., Webster, G.A., 1984. Prediction of creep crack growth from uniaxial creep data. Proc Roy Soc Lond A 1984 396, 183–197.

Oh, C.S., Kim, N.H., Kim, Y.J., Davies, C.M., Nikbin, K.M., Dean, D.W., 2011. Creep failure simulations of 316H at 550°C: Part I – a method and validation. Eng. Fract. Mech. 78, 2966–2977. https://doi.org/10.1016/j.engfracmech.2011.08.015.

Parker, J., 2017. Creep ductility considerations for high energy components manufactured from creep strength enhanced steels. Mater. A. T. High. Temp. 34 (2), 109–120. https://doi.org/10.1080/09603409.2016.1270720.

Parker, J., Brett, S., 2013. Creep performance of a grade 91 header. Int. J. Pres. Ves. Pip. 111–112, 82–88. https://doi.org/10.1016/j.ijpvp.2013.05.003.

Parker, J., Siefert, J., 2018. Metallurgical and stress state factors which affect the creep and fracture behavior of 9% Cr steels. Adv. Mater. Sci. Eng. 2018 https://doi.org/10.1155/2018/6789563. Article ID 6789563, 15 pages.

Parker, J., Siefert, J., 2020. Creep damage in long-term grade 91 steel component tests. Mater. A. T. High. Temp. 37, 425–433. https://doi.org/10.1080/09603409.2020.1813963.

Pétry, C., Lindet, G., 2009. Modelling creep behaviour and failure of 9Cr-0.5Mo-1.8W-VNb steel. Int. J. Pres. Ves. Pip. 86, 486–494. https://doi.org/10.1016/j.ijpvp.2009.03.006.

Rabotnov, Y.N., 1969. Creep Problems in Structural Members. North-Holland; 1969, Amsterdam, p. 836.

Ragab, R., Parker, J., Li, M., Liu, T., Sun, W., 2021. Modelling of a Grade 91 power plant pressurised header weldment under ultra super-critical creep conditions. Int. J. Pres. Ves. Pip. 192, 104389. https://doi.org/10.1016/j.ijpvp.2021.104389.

Review of Fabrication and In-Service Performance of a Grade 91 Header, 2013. EPRI, Palo Alto, CA, p. 3002001831.

Rice, J.R., Tracey, D.M., 1968. On the ductile enlargement of voids in triaxial stress fields. J. Mech. Phys. Solid. 17, 201–217. https://doi.org/10.1016/0022-5096(69)90033-7.

Shlyannikov, V., Tumanov, A., 2018a. Creep damage and stress intensity factor assessment for plane multi-axial and three-dimensional problems. Int. J. Solid Struct. 150, 166–183. https://doi.org/10.1016/j.ijsolstr.2018.06.009.

Shlyannikov, V., Tumanov, A., 2018b. Creep-fracture resistance parameters determination based on stress and ductility damage models. Fatig. Fract. Eng. Mater. Struct. 41, 2110–2129. https://doi.org/10.1111/ffe.12766.

Siefert, J.A., 2019. The Influence of the Parent Metal Condition on the Cross-Weld Creep Performance in Grade 91 Steel. PhD Thesis. Loughborough University. https://doi.org/10.26174/thess.lboro.8309882.v1 (Available on.

Siefert, J.A., Parker, J.D., Thomson, R.C., 2017. Factors contributing to heat affected zone damage in Grade 91 steel feature type cross-weld tests. In: Presented at the 4th International ECCC Creep & Fracture Conference. Dusseldorf, Germany, 10th-14th September 2017.

Spindler, M.W., 2004. The multiaxial creep ductility of austenitic stainless steels. Fatig. Fract. Eng. Mater. Struct. 27, 273–281. https://doi.org/10.1111/j.1460-2695.2004.00732.x.

Spindler, M.W., 2007. An improved method for calculation of creep damage during creep–fatigue cycling. Mater. Sci. Technol. 23 (12), 1461–1470. https://doi.org/10.1179/174328407X243924.

Takahashi, Y., Shigeyama, H., Siefert, J., Parker, J., 2018. Effect of simulated heat affected zone thermal cycle on the creep deformation and damage response of Grade 91 steel including heat-to-heat variation. In: Proceedings of the ASME 2018 Pressure Vessels and Piping Conference, July 15-20, 2018, Prague, Czech Republic, 2018. https://doi.org/10.1115/PVP2018-85102.

Takahashi, Y., Shigeyama, H., Siefert, J., Parker, J., 2019. A summary of 10 years research on Grade 91 and Grade 92 steel. Int. Conference Adv. High Temperature Mater. 60, 370–378. Nagasaki (Japan), October 21-24, 2019.

Webster, G.A., Nikbin, K.M., 2003. Finite element analysis of notched bar skeletal point stresses and dimensional changes due to creep *Fatigue*. & Fracture of Engineering Materials & Structures 27, 297–303. https://doi.org/10.1111/j.1460-2695.2004.00704.x.

Wen, J.F., Tu, S.T., 2014. A multiaxial creep-damage model for creep crack growth considering cavity growth and microcrack interaction. Eng. Fract. Mech. 123, 197–210. https://doi.org/10.1016/j.engfracmech.2014.03.001.

Wen, J.F., Tu, S.T., Gao, X.L., Reddy, J.N., 2013. Simulations of creep crack growth in 316 stainless steel using a novel creep-damage model. Eng. Fract. Mech. 98 (1), 169–184. https://doi.org/10.1016/j.engfracmech.2012.12.014.

Wen, J.F., Tu, S.T., Xuan, F.Z., Zhang, X.W., Gao, X.L., 2016. Effects of stress level and stress state on creep ductility: evaluation of different models. J. Mater. Sci. Technol. 32 (8), 695–704. https://doi.org/10.1016/j.jmst.2016.02.014.

Wen, W., Sun, W., Becker, A.A., 2019. A two-material miniature specimen test method and the associated inverse approach for high temperature applications, *Theor*. Appl. Fract. Mech. 99, 1–8. https://doi.org/10.1016/j.tafmec.2018.10.008.

Xu, Q., Barrans, S., 2003. The development of multiaxial creep damage constitutive equations for 0.5Cr-0.5Mo-0.25 V ferritic steel at 590° C. JSME Int. J. 46 (1), 51–59. https://doi.org/10.1299/jsmea.46.51.

Xu, Q., Lu, Z., Wang, X., 2017. Damage modelling: the current state and the latest progress on the development of creep damage constitutive equations for high Cr steels. Mater. A. T. High. Temp. 34 (3), 229–237. https://doi.org/10.1080/09603409.2017.1289613.

Yatomi, M., Nikbin, K.M., O'Dowd, N.P., 2003. Creep crack growth prediction using a damage based approach. Int. J. Pres. Ves. Pip. 80, 573–583. https://doi.org/10.1016/S0308-0161(03)00110-8.

Yatomi, M., Bettinson, A.D., O'Dowd, N.P., Nikbin, K.M., 2004. Modelling of damage development and failure in notched-bar multiaxial creep tests. Fatig. Fract. Eng. Mater. Struct. 27, 283–295. https://doi.org/10.1111/j.1460-2695.2004.00755.x.

Yatomi, M., Davies, C.M., Nikbin, K.M., 2008. Creep crack growth simulations in 316H stainless steel. Eng. Fract. Mech. 75, 5140–5150. https://doi.org/10.1016/j.engfracmech.2008.08.001.

Zhang, Y.C., Jiang, W., Tu, S.T., Zhang, X.C., Ye, Y.J., 2017. Creep crack growth behavior analysis of the 9Cr-1Mo steel by a modified creep-damage model. Mater. Sci. Eng. A 708, 68–76. https://doi.org/10.1016/j.msea.2017.09.112.

Zhang, Y., Chen, C., Jiang, W., Tu, S., Zhang, X., Li, F., 2020a. Evaluation of the creep crack growth behavior in 9Cr–1Mo steel under different stress conditions. Int. J. Pres. Ves. Pip. 188, 104174. https://doi.org/10.1016/j.ijpvp.2020.104174.

Zhang, W., Wang, X., Wang, Y., Yu, X., Gao, Y., Feng, Z., 2020b. Type IV failure in weldment of creep resistant ferritic alloys: I. Micromechanical origin of creep strain localization in the heat affected zone. J. Mech. Phys. Solid. 134 https://doi.org/10.1016/j.jmps.2019.103774.